

# Determining the Closed Flux Surface in a Helical Plasma in TOKASTAR-2 with an Electrostatic Probe

Hiromasa ITOU<sup>a)</sup>, Takaaki FUJITA, Hideki ARIMOTO, Atsushi OKAMOTO, Kenji MURAOKA, Ryoichi SUGIOKA, Kohei YASUDA, Ryoma YOKOYAMA, Masato MINOURA and Takahiro YAMAUCHI

Graduate School of Engineering, Nagoya University, Furo-cho, Chikusa-ku, Nagoya 464-8603, Japan

(Received 20 September 2017 / Accepted 7 March 2018)

The electron temperature and density were measured with an electrostatic probe in a helical plasma in the TOKASTAR-2 device in order to determine the location and the shape of the last closed flux surface (LCFS). The electron density inside the calculated LCFS was found to be higher in a helical plasma than in a plasma without a helical field when the electron-cyclotron-resonance layer was located inside the LCFS. Although errors in the manufacturing and installation of coils have been a concern, this result indicates that the LCFS formed in this device does not differ greatly from the calculated LCFS.

© 2018 The Japan Society of Plasma Science and Nuclear Fusion Research

Keywords: TOKASTAR, stellarator, flux surface, field-line tracing, electron orbit, triple-probe measurement

DOI: 10.1585/pfr.13.1402039

## 1. Introduction

The TOKASTAR-2 device is a low-aspect-ratio ( $A < 3$ ) tokamak-stellarator hybrid device [1]. Improvements in plasma position stability and suppression of disruption were shown by adding a helical field to the tokamak plasma [2–5]. The main research objective of TOKASTAR-2 is to study these effects of the helical field on the tokamak plasma and to investigate the effect of increasing the rotational transform by inducing a plasma current in the helical plasma, both in a low  $A$  regime.

The present TOKASTAR-2 device has a stellarator coil system that produces closed magnetic flux surfaces without any plasma current. The closed flux surfaces were not formed with the original stellarator coil system but formed by adding additional helical field (AHF) coils in 2012. The AHF coils were designed to produce closed flux surfaces based on a magnetic field-line tracing analysis [6]. The effect of the helical field on the radial position of the tokamak plasma in TOKASTAR-2 was subsequently determined from an internal magnetic field measurement [7] and by imaging with a high-speed camera [8]. In contrast, adding a helical field to the toroidal field has only a small effect on an RF-heated plasma without a plasma current [9]. This may imply that the location and shape of the closed magnetic flux surfaces may deviate significantly from the calculated ones due to errors in the manufacturing and installation of the coils. The main purpose of the present study is to measure the electron temperature and density with an electrostatic probe and to determine the location and shape of the flux surfaces experimentally. We

anticipate improvements in confinement with the closed flux surfaces. Direct measurements of the flux surfaces with an electron gun are also in preparation [10].

## 2. The TOKASTAR-2 Device

Figure 1 shows a schematic view of the TOKASTAR-2 device. It contains eight toroidal field (TF) coils, three blocks of ohmic heating (OH) coils, a pair of pulsed vertical field (PVF) coils, a pair of static vertical field (VF) coils, two outboard helical field (HF) coils, four AHF coils, and two shape control (SC) coils. The TOKASTAR-2 device can be operated using the tokamak coil system and the helical coil system independently. Two sets of an HF coil and AHF coils are installed in the toroidal direction and then helical fields with toroidal mode numbers  $n = 1$  or  $2$  can be generated by changing the coil connections. In this study we used an  $n = 2$  field. Microwaves at a frequency of

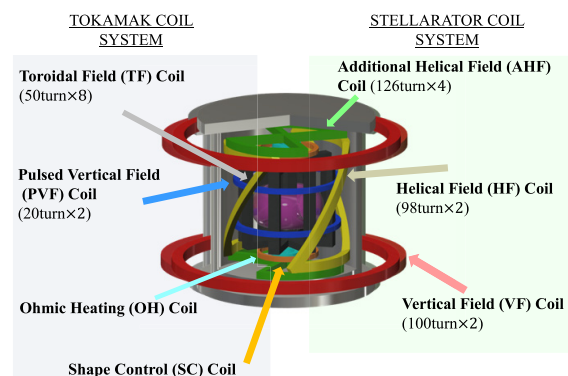


Fig. 1 Schematic view of the TOKASTAR-2 device.

author's e-mail: fujita@energy.nagoya-u.ac.jp

<sup>a)</sup> The current affiliation is Mitsubishi Hitachi Power Systems.

2.45 GHz is injected to generate plasma through the fundamental electron cyclotron resonance (ECR) at a magnetic field strength of 0.0875 T.

### 3. Triple-Probe Measurements

To determine the electron temperature and density, we used a triple-probe measurement. In this method, three electrodes (probe tips) are inserted into the plasma, and the probe currents and potentials are measured. Electrostatic triple-probe measurements are well suited for plasmas with rapidly varying parameters, since they allow simultaneous measurements of the plasma parameters without sweeping the voltage.

The probe tips consist of three parallel tungsten wires 2.5 mm long and 0.6 mm in diameter. They are separated by a distance of 1 mm as shown in Fig. 2. Each wire is covered by a ceramic tube and is connected to a coaxial cable. Figure 3 shows a side view of the TOKASTAR-2. The plasma is generated between the inner walls of the TF coils, which have dimensions of  $6.5 \text{ cm} \leq R \leq 18 \text{ cm}$  in the radial direction and  $-13 \text{ cm} \leq Z \leq 13 \text{ cm}$  in the vertical direction. A poloidal limiter made of stainless steel was newly installed in April 2016; it confines the plasma between  $R = 7.5 \text{ cm}$  and  $17.2 \text{ cm}$  and between  $Z = -12 \text{ cm}$  and  $12 \text{ cm}$ . The triple probe is inserted from one of the four ports on the side of the vessel and can be extended radially into the plasma over the range  $6 \text{ cm} \leq R \leq 24 \text{ cm}$ . The port for the probe is located at the toroidal angle  $\phi = 90^\circ$ , while the port for the microwave injection is located on the opposite side, at  $\phi = 270^\circ$ . The angle  $\phi = 0^\circ$  corresponds to the center of the viewing port, which is located in the middle between adjacent TF coils.

Figure 4 shows the electrical circuits for the triple-probe measurement. We apply a fixed voltage between probe tips  $P_1$  and  $P_2$  and measure the ion saturation current flowing through them while simultaneously measuring the electric potential difference  $V_{23}$  between probe tips  $P_2$  and  $P_3$ . The electron temperature  $T_e$  in eV is obtained from the electric potential difference  $V_{23}$  in V as  $T_e = V_{23}/\ln 2$ , and the electron density  $N_e$  is given by [11]

$$N_e = \frac{I_{is}}{0.61 \cdot e \cdot S} \sqrt{\frac{M_+}{e \cdot T_e}},$$

where  $I_{is}$  is the ion saturation current,  $M_+$  is the mass of the ion, and  $S$  is the surface area of the probe tip. The voltage between probe tips  $P_1$  and  $P_2$  must be large enough to measure the ion saturation current, but too large a voltage results in a larger density than the values measured by a single or a double probe. We determined the appropriate voltage for this study to be 35 V after measuring the I-V characteristics with single and double probes. At this voltage, the current flowing through probe tips  $P_1$  and  $P_2$  is in the ion-saturation-current regime and the density obtained is close to that obtained with the single and double probes.

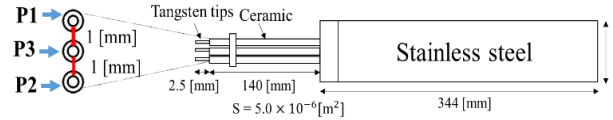


Fig. 2 Drawing of the triple probe.

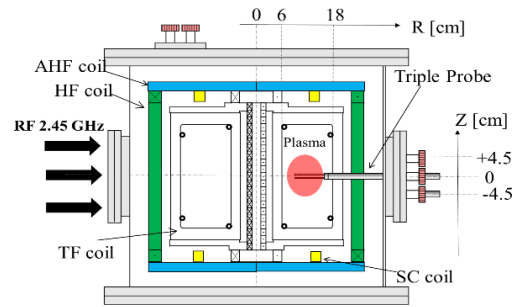


Fig. 3 Side view of TOKASTAR-2.

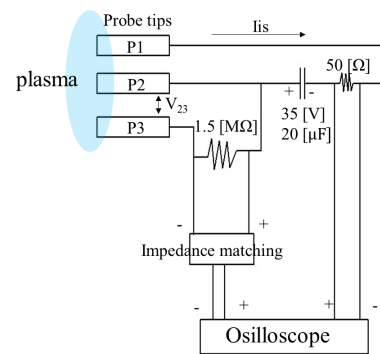


Fig. 4 Electrical circuits for the triple probe measurement.

### 4. Calculation of the Last Closed Flux Surface and Electron Orbits

We calculated the shape of the last closed flux surface (LCFS) using the HSD code [12]. In that code, a field line is traced by using the Biot-Savart law. Figure 5 shows the calculated LCFSs for various TF-coil current conditions. For the present calculations, the HF-coil current was 2.5 kA-turn, the AHF-coil current was 2.9 kA-turn and the VF-coil current was 0.15 kA-turn. Since the helical field is not axisymmetric, the poloidal cross section of the flux surface varies slightly in the toroidal direction. In this paper we show the cross sections at the probe port position or at the toroidal angle  $\phi = 90^\circ$ . The shape of the LCFS is elongated in the vertical direction, at all toroidal angles, and the position changes with the TF-coil current. Since no helical field coils are located on the high-field side, a vertical field is needed to define the magnetic axis and produce closed flux surfaces. The magnetic axis is formed where the effective vertical field generated by the HF and AHF

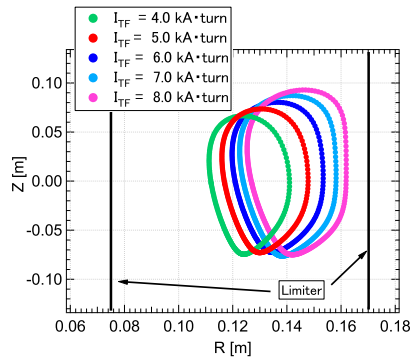


Fig. 5 Calculated last closed magnetic surfaces for various TF-coil currents from 4 kA·turn to 8 kA·turn. The HF-, AHF- and VF-coil currents are fixed. The vertical black lines denote the inner and outer limiters.

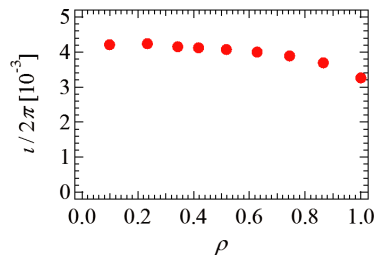


Fig. 6 Calculated radial profile of the rotational transform. The TF-coil current is 8 kA·turn. The horizontal axis denotes the normalized minor radius

coils is cancelled by the axisymmetric vertical field generated by the VF coils. When the toroidal field is higher, the effective vertical field generated by the HF and AHF coils decreases and then the magnetic axis moves outward to a position where the vertical field is lower. The radial profile of the rotational transform is shown in Fig. 6. The small rotational transform is due to the weak helical field at the inner side of the torus where no helical field coils are located.

We also calculated the orbit of the electron guiding center with the HSD code in order to determine how much the electron orbits are shifted from the closed flux surfaces. The energy and the initial pitch angle (the angle between the magnetic-field-line vector and the velocity vector) of the electrons are varied in the calculation.

Figure 7 shows the results of the pitch-angle scan. In each case, the electron was emitted at  $Z = 0$  cm,  $R = 13.7$  cm and  $\phi = 90^\circ$ , and the electron energy was 10 eV, which corresponds to the typical electron temperature in the experiment. The TF-coil current was 8.0 kA·turn. The starting point is located on the ECR layer where the electrons are heated by microwaves. Here the magnetic field generated by the TF coils at  $\phi = 90^\circ$  was calculated from the Biot-Savart law, without assuming toroidal symmetry. This field was used to determine the position of the

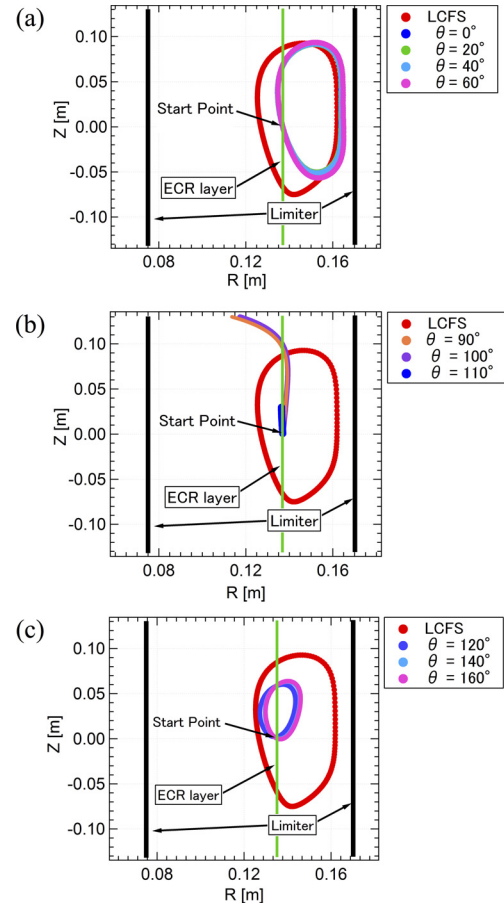


Fig. 7 Dependence on the pitch angle  $\theta$  of the orbit of electrons with 10 eV. The red lines denote the last closed flux surfaces, the green vertical lines denote the electron-cyclotron-resonance layers and the vertical black lines denote the inner and outer limiters. (a)  $\theta = 0^\circ, 20^\circ, 40^\circ, 60^\circ$ . (b)  $\theta = 90^\circ, 100^\circ, 110^\circ$ . (c)  $\theta = 120^\circ, 140^\circ, 160^\circ$ . The TF-coil current is 8 kA·turn. The start point is located at  $R = 137$  mm and  $Z = 0$ .

ECR layer, since a large toroidal field ripple ( $\sim 10\%$ ) exists around  $R = 14$  cm [13]. The helical field is about 4 mT at  $R = 12$  cm, which is about 5% of the toroidal field strength. The helical field is nearly perpendicular to the toroidal field and thus the magnitude of the total field is only 0.1% larger than the toroidal field. The shift in the ECR position due to the helical field is therefore about 0.1 mm, which is negligible. When the pitch angle  $\theta$  is in the range  $0^\circ \leq \theta < 65^\circ$ , the electrons are confined as shown in Fig. 7 (a). The electron orbits are shifted outward and the sizes of the orbits are smaller than the calculated LCFS. The electron orbit depends only weakly on the pitch angle in this range.

When the pitch angle is in the range  $65^\circ \leq \theta < 115^\circ$ , the electrons are not confined within the closed flux surface as shown in Fig. 7 (b). The electrons with  $\theta = 90^\circ - 100^\circ$  collide with the upper part of the TF coil. When the pitch angle is in the range  $115^\circ \leq \theta \leq 180^\circ$ , the electrons are confined within the closed flux surface as shown

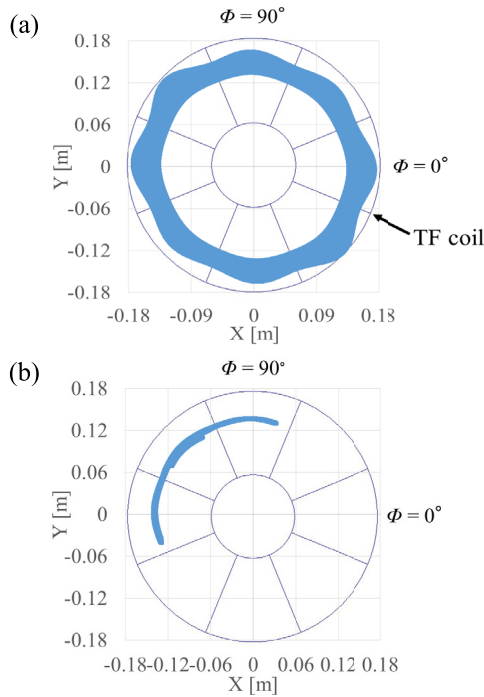


Fig. 8 Orbits of electrons as viewed from the top of TOKASTAR-2 for an electron with (a) a pitch angle of  $0^\circ$  and (b) a pitch angle of  $70^\circ$ .

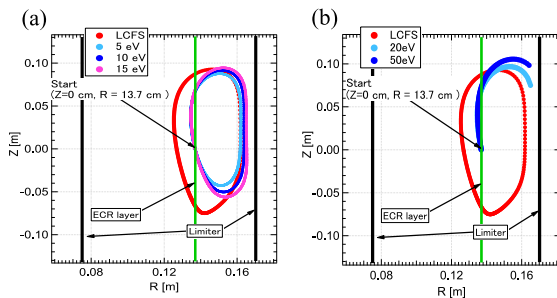


Fig. 9 Dependence on the energy of the electron orbit. In (a) the electron energy is 5, 10 and 15 eV and in (b) it is 20 and 50 eV.

in Fig. 7 (c). However, in these cases the size of the orbit is much smaller than the LCFS.

Figure 8 shows the orbits of electrons with the pitch angles of  $0^\circ$  and  $70^\circ$ , as viewed from the top of TOKASTAR-2. Electrons with a pitch angle of  $0^\circ$  circle the torus around the major axis, namely are the passing particles (Fig. 8 (a)). Conversely, electrons with a pitch angle of  $70^\circ$  are trapped by the ripple of the helical field (Fig. 8 (b)). Electrons with pitch angles in the range  $65^\circ \leq \theta \leq 105^\circ$  are trapped and then are lost quickly.

Figure 9 shows the results by varying the electron energy. In these calculations, the pitch angle was  $0^\circ$ , and the electron was emitted at  $Z = 0$  cm,  $R = 13.7$  cm, and  $\phi = 90^\circ$ . The TF-coil current was 8.0 kA-turn. Electrons with energies in the range 5 - 16 eV are confined as shown

in Fig. 9 (a). The electron orbits are almost the same over this energy range. However, the electrons with energies greater than 17 eV are not confined and collide with the outer limiter. The collision occurs at a toroidal angle of  $0^\circ$ , so the orbit does not reach the outer limiter in Fig. 9 that shows the cross section at the toroidal angle of  $90^\circ$ . From these results, we have found that some electrons with typical energies are confined by the helical field, and their orbits are not greatly different from the flux surfaces, assuming no errors in the manufacturing and installation of the coils.

## 5. Experimental Results

In order to determine the location and the shape of the closed flux surfaces from the density and temperature measurements, we have compared the results for plasmas with and without closed magnetic-field surfaces in the experiment. The closed flux surfaces were generated by using the TF, HF, AHF, and VF coils while no closed flux surfaces were generated when using the TF coil alone. In this paper, we term the former a “helical plasma” and the latter an “ECH plasma.” The HF-, AHF-, and VF-coil currents were kept constant, while the TF-coil current was changed during the microwave injection; the TF coils are connected to a pulsed power supply with capacitor banks while the HF, AHF, and VF coils are connected to steady power supplies. We used nitrogen as the working gas, with a typical gas filling pressure of 0.4 mTorr. The injected microwave power was about 1.2 kW. We measured the electron temperature and density in the ECH plasma and in the helical plasma by using the triple probe. The ECR layer position changed in accordance with the changes in the TF-coil current. The ECH plasma and the helical plasma were generated at the point in time when the ECR layer reached the inner wall of the TF coils, at  $t = 1.2$  ms in this experiment, and the plasmas disappeared when microwave injection was terminated at  $t = 8$  ms. After plasma generation, the ECR layer moved outward and entered the LCFS. After the peak of the TF-coil current around  $t = 2.8$  ms, the ECR layer moved inward again and exited the LCFS. This change in the heating-power profile can also be utilized to determine the LCFS, in addition to comparing the helical-plasma results to the ECH plasma with no LCFS.

Figure 10 shows the radial profiles of the electron density at  $Z = 0$  cm at three time slices. In the ECH plasma (red line), which has no closed flux surfaces, the electron density peaks at  $R = 17$  cm between  $t = 3$  ms and 6 ms, and the density decreases beyond the poloidal limiter. The reason for this density distribution seems to be that the plasma drifted outward due to  $E \times B$  drift, and  $R = 17$  cm is the outermost position where the field line can circle in the toroidal direction. On the other hand, the electron density in the helical plasma (blue line) was larger than that of the ECH plasma inside the LCFS (pink vertical lines) at  $t = 3$  ms and 4 ms, when the ECR layer was located inside

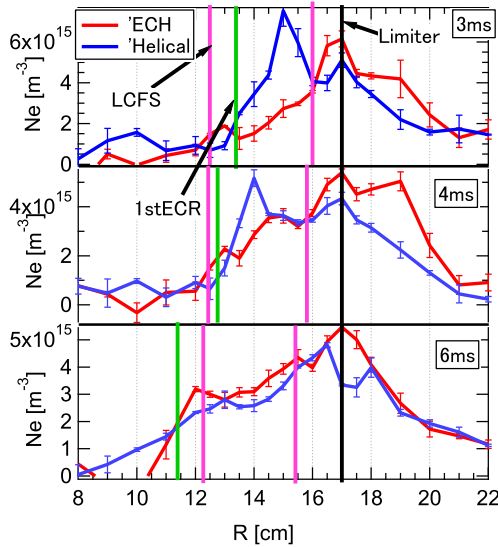


Fig. 10 Radial profiles of the electron density at  $Z = 0$  cm at three time slices. The red and blue lines denote the ECH plasma and the helical plasma, respectively. The pink vertical lines denote the radial positions of the LCFS at  $Z = 0$  while the green vertical lines denote the position of the ECR layer.

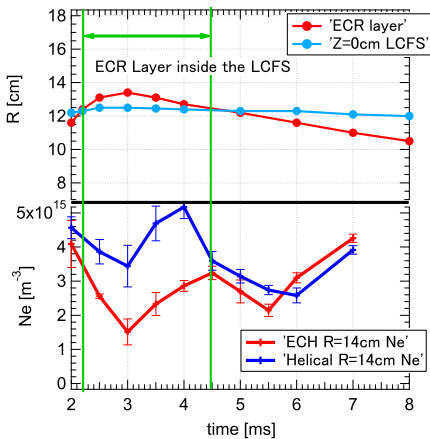


Fig. 11 (Top) Time evolution of the radial position of the inner edge of the LCFS and the ECR layer. (Bottom) Time evolution of the electron density at  $R = 14$  cm in the ECH and the helical plasmas.

the calculated LCFS. This seems to indicate an improvement in plasma confinement with the closed magnetic surfaces formed in the helical plasma. The locations where the density of the helical plasma exceeds that of the ECH plasma also agree roughly with the range of positions inside the calculated LCFS.

The time evolution of the same discharges is shown in Fig. 11. The top panel shows the time evolution of the radial positions of the LCFS and the ECR layer on the mid-plane. The bottom panel shows the time evolution of the electron density at  $R = 14$  cm, which is inside the LCFS.

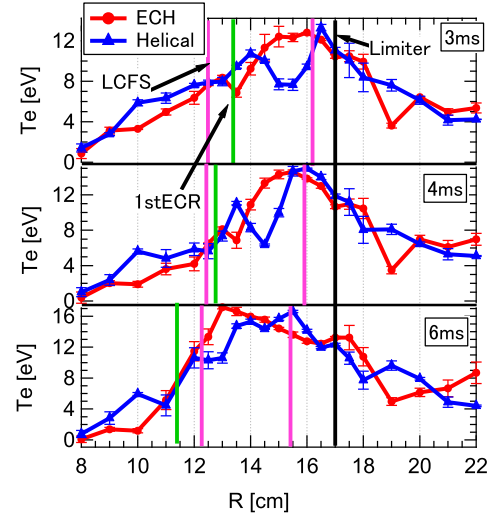


Fig. 12 Radial profiles of the electron temperature at  $Z = 0$  cm at three time slices.

The density in the helical plasma was larger than that in the ECH plasma during the period when the ECR layer was located inside the LCFS (between 2 ms and 4.5 ms). In contrast, after the ECR layer position left the LCFS, the electron densities in both the helical plasma and the ECH plasma are almost identical.

Figure 12 shows the radial profiles of the electron temperature at  $Z = 0$  cm. Although the electron density in the helical plasma was higher inside the LCFS than that in the ECH plasma, the electron temperature in the helical plasma was somewhat lower than that in the ECH plasma inside the LCFS. A possible reason may be that the energy injected by the microwaves was mainly used to ionize the gas, so the electrons were not accelerated enough to reach a high temperature, since both the ECH and the helical plasmas in TOKASTAR-2 are weakly ionized.

## 6. Summary

Using an electrostatic probe, we have measured the electron temperatures and densities of a helical plasma in TOKASTAR-2. We calculated the electron orbits and the last closed flux surface (LCFS) under typical experimental conditions in TOKASTAR-2 using a field-line tracing code. We found that some electrons with typical energies are confined by the helical field and that their orbits do not differ greatly from the flux surfaces, if we assume no errors in the manufacturing and installation of coils. Inside the calculated LCFS, we found that the density of a helical plasma was higher than that of an ECH plasma, which does not have closed flux surfaces, and that the density peak region was formed when the electron-cyclotron-resonance layer was inside the LCFS. The region where the density in the helical plasma was larger than that in the ECH plasma agrees roughly with the calculated LCFS positions. This result indicates that the LCFS formed in this device does

not differ greatly from the calculated LCFS. The electron temperature in the helical plasma was somewhat lower than that in the ECH plasma inside the LCFS, possibly because the injected energy was used mainly to ionize the gas, so the electrons were not accelerated enough to reach a high temperature.

## Acknowledgments

This work was performed with the support and under the auspices of the NIFS Collaboration Research program (NIFS14KOAP027) including the NIFS Joint Use Program of Measurement Instruments.

- [1] K. Yamazaki, Y. Taira, T. Oishi *et al.*, J. Plasma Fusion Res. SERIES **8**, 1044 (2009).
- [2] H. Ikezi, K.F. Schwarzenegger and C. Ludescher, Phys. Fluids **22**, 2009 (1979).
- [3] K. Sakurai and S. Tanahashi, J. Phys. Soc. Jpn. **49**, 759 (1980).
- [4] W VII-A TEAM, Nucl. Fusion **20**, 1093 (1980).
- [5] J. Fujita *et al.*, Plasma Physics and Controlled Nuclear Fusion Research (Proc. 8th Int. Conf., Brussels, Belgium, 1980) Vol.1, p.209.
- [6] M. Hasegawa, K. Yamazaki, H. Arimoto *et al.*, Plasma Fusion Res. **7**, 2402116 (2012).
- [7] T. Ueda, H. Arimoto, T. Fujita *et al.*, Plasma Fusion Res. **10**, 3402065 (2015).
- [8] T. Sakito, H. Arimoto, T. Fujita *et al.*, Plasma Fusion Res. **11**, 2402074 (2016).
- [9] T. Sakito, H. Arimoto, T. Fujita *et al.*, Plasma Fusion Res. **10**, 3402033 (2015).
- [10] Y. Shimooka, H. Arimoto, T. Fujita *et al.*, Plasma Fusion Res. **11**, 2402110 (2016).
- [11] S.L. Chen and T. Sekiguchi, J. Appl. Phys. **36**, 2363 (1965).
- [12] K. Yamazaki, O. Motojima and M. Asao, Fusion Technol. **21**, 147 (1992).
- [13] T. Oishi, K. Yamazaki, K. Okano *et al.*, J. Plasma Fusion Res. SERIES **9**, 69 (2010).